HHS Public Access

Author manuscript

Cell. Author manuscript; available in PMC 2017 March 24.

Published in final edited form as:

Cell. 2016 March 24; 165(1): 207–219. doi:10.1016/j.cell.2016.01.027.

Spinal inhibitory interneuron diversity delineates variant motor microcircuits

Jay B. Bikoff[1,*], **Mariano I. Gabitto**[1], **Andre F. Rivard**[2], **Estelle Drobac**[3], **Timothy A. Machado**[1], **Andrew Miri**[1], **Susan Brenner-Morton**[1], **Erica Famojure**[1], **Carolyn Diaz**[1], **Francisco J. Alvarez**[2], **George Z. Mentis**[3], and **Thomas M. Jessell**[1,*]

1

2

3

SUMMARY

Animals generate movement by engaging spinal circuits that direct precise sequences of muscle contraction, but the identity and organizational logic of local interneurons that lie at the core of these circuits remain unresolved. Here we show that V1 interneurons, a major inhibitory population that controls motor output, fractionate into highly diverse subsets on the basis of the expression of nineteen transcription factors. Transcriptionally defined V1 subsets exhibit distinct physiological signatures and highly structured spatial distributions with mediolateral and dorsoventral positional biases. These positional distinctions constrain patterns of input from sensory and motor neurons, arguing that interneuron position is a determinant of microcircuit organization. Moreover, V1 diversity indicates that different inhibitory microcircuits exist for motor pools controlling hip, ankle, and foot muscles, revealing a variable circuit architecture for interneurons that control limb movement.

INTRODUCTION

Animals interact with the world through movement, translating intent into action through the transformation of neural activity into the orderly contraction of muscles. The spinal circuits assigned to the control of limb movement take advantage of interneurons that drive motor

*Correspondence: tmj1@cumc.columbia.edu (T.M.J.), jb3098@cumc.columbia.edu (J.B.B.).

AUTHOR CONTRIBUTIONS

J.B.B. and T.M.J. devised the project. M.I.G., A.F.R., and E.D. contributed equally to this work. J.B.B. performed molecular, genetic, and anatomical experiments, with assistance from E.F. and C.D. M.I.G. contributed to the statistical analysis of V1 diversity. A.F.R. and F.J.A. characterized the firing features of V1 subsets. E.D. and G.Z.M. performed electrophysiological experiments in the spinal cord-hindlimb preparation. T.A.M. and A.M. helped analyze V1 spatial distributions, and S.B.M. developed antibodies. J.B.B. and T.M.J. wrote the manuscript, with input from all authors.

SUPPLEMENTAL INFORMATION

Supplemental Information includes Supplemental Experimental Procedures, seven figures, and one table, and can be found with this article online at:

neurons in precisely timed sequences, and that serve as relays for sensory feedback and descending command pathways (Arber, 2012; Windhorst, 2007). Defining the circuit logic through which local interneurons direct motor output is therefore a central issue in the neural control of movement.

Inhibitory interneurons have major roles in shaping spinal motor output, through the formation of local networks with highly selective synaptic input and output connectivity (Goulding et al., 2014). Electrophysiological studies have provided insight into the organizational logic of mammalian inhibitory microcircuits, notably those mediating feedforward, reciprocal, and feedback inhibition (Jankowska, 1992). GABAergic interneurons mediate presynaptic inhibition of sensory input, glycinergic interneurons control the reciprocal inhibition of flexor/extensor antagonists, and glycinergic and/or GABAergic Renshaw interneurons mediate the recurrent inhibition of motor neurons (Baldissera et al., 1981). The neuronal diversity implied by these physiological descriptions has been complemented by the molecular delineation of four cardinal classes of ventral spinal interneurons, termed V0 to V3 interneurons, each possessing a distinctive transcription factor character and different patterns of local connectivity (Briscoe et al., 2000).

Despite advances in elucidating the wiring of spinal motor systems, the organization of local circuit interneurons remains obscure. At its core, defining the organizing principles of spinal motor circuitry depends on determining the diversity of discrete interneuron subtypes that nucleate circuits for limb movement. In much the same way that limb-innervating motor neurons acquire diverse pool identities, cardinal interneuron classes defined by transcriptional character may fragment into multiple subtypes. Moreover, different physiological subtypes of interneurons appear to occupy stereotypic settling positions within the intermediate and ventral spinal cord (Alvarez and Fyffe, 2007; Hultborn et al., 1971). Nevertheless, it remains unclear whether the construction of interneuronal circuits takes advantage of distinctions in neuronal position when establishing local connectivity, a precedent set by the role of motor neuron position in establishing stereotypic patterns of proprioceptive input (Sürmeli et al., 2011). It is also uncertain whether the local circuits that control motor output adhere to a canonical wiring diagram, reiterated for each motor pool.

To gain insight into the organization of inhibitory circuits for motor control we have analyzed diversity and connectivity within the V1 interneuron population. V1 interneurons express the homeodomain transcription factor En1, and use GABA and/or glycine as inhibitory neurotransmitters (Benito-Gonzalez and Alvarez, 2012; Saueressig et al., 1999). This set constitutes over one third of all inhibitory interneurons in the ventral spinal cord, and includes all Renshaw and many reciprocal inhibitory interneurons (Sapir et al., 2004; Zhang et al., 2014). Genetic ablation of V1 neurons slows the speed of rhythmic locomotor output and perturbs flexor/extensor alternation (Gosgnach et al., 2006; Zhang et al., 2014). But in the absence of information about the diversity and connectivity of component V1 subtypes, it has not been possible to resolve the circuit logic that underlies aberrant motor behavior.

In this study we use molecular genetic approaches, and in an accompanying paper statistical analysis (Gabitto et al., 2016), to delineate the extent and consequences of diversity within the V1 interneuron population. This combined analysis reveals that V1 interneurons can be fragmented into fifty transcriptionally defined subtypes. V1 subpopulations exhibit distinct physiological signatures and settle in highly localized positions along both the mediolateral and dorsoventral axes of the neonatal spinal cord, a feature that constrains patterns of sensory and motor input. Moreover, the wiring diagram of inhibitory interneuron microcircuits differs for motor pools innervating hip, ankle, and foot muscles, a feature likely to reflect differences in the biomechanical properties of individual muscles.

RESULTS

Transcriptional Diversity of V1 Inhibitory Interneurons

To explore the diversity of spinal inhibitory interneurons we compared gene expression profiles for $En1^+$ V1 and $Ptf1a^+$ dI4/dIL^A interneurons (Glasgow et al., 2005; Sapir et al., 2004) (Figure 1A). We reasoned that a comparison of these two inhibitory populations, which settle at different dorsoventral positions and contact distinct postsynaptic targets, could reveal genes that fractionate the parental V1 and dI4/dIL^A populations, while excluding generic inhibitory markers. We focused this analysis on transcription factors (TFs), given their roles in specifying neuronal subtype identity (Dalla Torre di Sanguinetto et al., 2008).

V1 and dI4/dIL^A interneurons were isolated by fluorescence-activated cell sorting, from spinal cords dissociated from *En1::Cre; Rosa.lsl.eYFP* and *Ptf1a::Cre; Rosa.lsl.eYFP* mice respectively. Microarrays were performed at e12.5, p0, and p5 - a developmental window that covers the emergence of interneuron identity and the formation of synaptic connections (Figures 1B,C and S1A-C). Comparative microarray analysis identified 56 genes that encoded TFs with a >3-fold enrichment in V1 interneurons (mean V1:dI4 enrichment: 74.5; range: 3.1 to 930-fold; $p \leq 0.02$, one-way ANOVA) at one or more developmental stages, and 160 TF genes with a >3-fold enrichment in dI4/dIL^A interneurons (mean dI4:V1 enrichment: 38.5; range: 3.1 to 784-fold; $p \leq 0.02$, one-way ANOVA). In this study, we focus on diversity within the parental V1 interneuron population.

Analysis of gene expression databases revealed that 32 of the 56 V1 TFs exhibited mosaic expression in the embryonic (e11.5-e15.5) or neonatal (p4) ventral spinal cord (Figure S1A). Two additional genes, *MafA* and *Prox1*, exhibit scattered expression in the ventral spinal cord, and were included in subsequent analyses. From these 34 candidates, we focused on 19 TFs for which we were able to generate (FoxP1, FoxP2, FoxP4, Lmo3, MafA, Nr3b2, Nr4a2, Nr5a2, Otp, Pou6f2, Prdm8, and Sp8) or obtain (Bhlhb5, MafB, Nr3b3, Oc1, Oc2, Prox1, and Zfhx4) antibodies (Figure S1D-O; see Supplemental Information for description of antibodies).

To evaluate the prevalence of these 19 TFs within the parental V1 population we marked V1 interneurons by LacZ expression in *En1::Cre; Tau.lsl.nLacZ* (*En1.nLacZ*) mice, and performed dual immunohistochemical analysis with antibodies directed against LacZ and each TF individually. V1 interneurons arise from the p1 progenitor domain between e9.5 -

e12.5 and undergo migration to their final settling position during embryogenesis (Matise and Joyner, 1997). We therefore focused our analysis on p0 lumbar spinal cord, when initial specification and migration is complete and before extinction of expression of many developmentally regulated TFs (Benito-Gonzalez and Alvarez, 2012). All 19 TFs were expressed in subsets of V1 interneurons (Figures 2A and S2A), with the incidence of expression ranging from 5% (MafA) to 74% (Lmo3) of the parental V1 population (Figure 2B). Conjoint exposure to antibodies directed against 14 of these TFs marked > 90% of V1 interneurons in p0 lumbar spinal segments, indicative of near-complete coverage of the parental V1 population (Figure 2C). In addition, 12 of the 19 V1 TFs were expressed within subsets of V2a interneurons (Figure S2C; threshold: 3%; range: 3-62% of parental V2a interneurons), indicating that this set of TFs reveals diversity in both V1 inhibitory and V2a excitatory interneurons.

We estimated the number of neuronal types within the parental V1 population through application of a Bayesian sparse linear regression algorithm that assigns V1 interneuron cell types on the basis of TF expression and settling position (Gabitto et al, 2016). The extent of co-expression was determined for binary TF combinations, with each pairing gated to $LacZ^+$ neurons in p0 *En1.LacZ* mice (Figure 2D). This analysis assigns 50 ± 2 V1 interneuron cell types, some defined by as many as 9 TFs (Gabitto et al., 2016). Four TFs - FoxP2, MafA, Pou6f2, and Sp8 - delineate non-overlapping clades that comprise 64% of the parental V1 population at p0, with each clade containing multiple cell types (Figures 2C,E and S2D). This combination of experimental observation and statistical inference therefore defines the extent of V1 diversity and its hierarchical organization.

Spatial Organization of V1 Interneuron Subpopulations

We considered whether V1 cell types are clustered in stereotypic settling patterns. Since individual V1 cell types are defined by as many as 9 TFs (Gabitto et al, 2016), it is not practical to delineate them on the basis of their complete transcriptional profile. We therefore assessed the spatial distributions defined by each of the 19 V1 TFs individually (Figure S3A) or in a few cases by the superimposition of two TFs (Figure S3B). These larger sets of V1 interneurons, termed “composite groups”, are predicted to contain multiple V1 cell types (Figure S3C). Any spatial restriction of these larger V1 interneuron groups would imply clustering of individual V1 types.

We first examined the single instance in which an inferred V1 cell type can be delineated by the co-expression of just two TFs, Nr5a2 and Pou6f2. With respect to the parental V1 population, which extends ~400 μm along the dorsoventral (D/V) and mediolateral (M/L) axes in p0 lumbar spinal cord, the $V1^{Nr5a2/Pou6f2}$ cell type revealed a markedly confined settling position (Figure 3A,B). Each of the V1 composite groups also occupied a domain more restricted than that of the parental V1 distribution profile (Table S1, $p < 0.001$ by one-tailed Monte Carlo test; single TF-gated fractional area (F_a) range: 0.217 to 0.855, dual TF-gated F_a range: 0.085 to 0.365). By extension, it follows that the individual V1 cell types contained within these composite groups will also be clustered.

We examined the degree to which subsets of V1 interneurons settle at distinct positions in the ventral spinal cord, focusing initially on the four primary V1 clades. The $V1^{MafA}$,

$V1^{Pou6f2}$, and $V1^{Sp8}$ clades showed discrete distributions along the D/V and M/L axes (Figure 3C,D and Table S1), whereas the FoxP2 clade occupies a broader domain (Figure S3A, $F_a = 0.855$). $V1^{Pou6f2}$ interneurons fractionated into medial $Nr5a2^+$ and lateral $Lmo3^+$ interneurons, with 93% mutual exclusion, demonstrating segregation within the members of a single clade (Figure 3E). Similarly, the $V1^{Prdm8}$ composite group fractionated into dorsal $Sp8^+$ and ventral $FoxP4^+$ subsets (Figure 3F). The mean position of V1 cell types and composite groups at L3-L5 levels of lumbar spinal cord was constant between animals (Figure 3H). Moreover, V1 settling positions are stable from e15.5 to p20, an indication that V1 neuronal clustering is not a transient reflection of developmental stage (Figure S4A-B).

The ventral location of the $V1^{MafA}$ clade prompted us to examine its relationship to Renshaw ($V1^R$) interneurons. This V1 subtype occupies the most ventral region of the parental V1 distribution, expresses the transcription factors Oc1, Oc2, and MafB and the calcium binding protein calbindin, and mediates recurrent inhibition of motor neurons (Alvarez and Fyffe, 2007; Stam et al., 2012). Analysis of $V1^R$ interneurons at e13.5, shortly after their initial specification and migration within the ventral spinal cord, demonstrated the existence of $MafA^+$ and $MafA^-$ $V1^R$ subsets, with 61.6 ± 5.8% of $V1^R$ interneurons expressing MafA (Figure S2E,F). A similar molecular diversity is evident at p0, potentially corresponding to descriptions of morphological heterogeneity amongst $V1^R$ interneurons (Fyffe, 1990). Conversely, ~20% of $V1^{MafA}$ interneurons are located > 200 μm from the ventral edge of the spinal cord, a dorsal position that effectively excludes them as $V1^R$ interneurons. Thus, $V1^R$ and $V1^{MafA}$ interneurons are not co-extensive - while many $V1^R$ neurons are contained within the $V1^{MafA}$ clade, others comprise ventral V1 interneurons distinct from the $V1^{MafA}$ clade as well as more dorsal $V1^{FoxP2}$, $V1^{Pou6f2}$, or $V1^{Sp8}$ clades.

$V0_C$ interneurons exhibit rostrocaudal variation in transmitter phenotype and connectivity (Zagoraiou et al., 2009), prompting us to determine whether neurons in $V1^{Pou6f2}$ and $V1^{Sp8}$ clades exhibit rostrocaudal distinctions in settling position. The overall positional bias of $V1^{Pou6f2}$ and $V1^{Sp8}$ interneurons was maintained at single segmental levels between L3 and L5 (Figure S4C-E). Nevertheless, minor differences in the settling position of $V1^{Pou6f2}$ and $V1^{Sp8}$ clades were evident, with a ventromedial shift for $V1^{Pou6f2}$ and a ventrolateral shift for $V1^{Sp8}$ at progressively more caudal lumbar levels (Figures 3G and S4D,E; see also Figure 5C,E). Thus, V1 interneuron settling position exhibits overall constancy, albeit with subtle differences along the lumbar rostrocaudal axis.

In total, this analysis of V1 identity and settling position identifies numerous spatially discrete V1 subpopulations, seven of which are illustrated (Figure 3I, see also Gabitto et al, 2016). These seven clusters represent ~44% of the parental V1 population and comprise 39 inferred cell types. The extent of V1 interneuron diversity goes beyond that recognized previously for interneuron populations in the mammalian CNS (Sanes and Masland, 2015).

V1 Clades Contain Physiologically Distinct Interneuron Subsets

To determine whether molecular distinctions in V1 identity reflect differences in interneuron physiology, we analyzed the electrophysiological properties of neurons in $V1^{FoxP2}$ and $V1^{Pou6f2}$ clades, as well as $V1^R$ interneurons, in a spinal cord slice preparation at p10-p14. To label neurons in the $V1^{FoxP2}$ clade, we generated *FoxP2::Flpo* transgenic mice, and used

an intersectional genetic strategy in which *En1::Cre*; *FoxP2::Flpo; RCE.dual.GFP* mice selectively express GFP in $V1^{FoxP2}$ interneurons (Figure S5A-C). To identify both the $V1^{Pou6f2}$ clade and $V1^{R}$ interneurons, we used *MafB::GFP; En1::Cre; Rosa.lsl.tdT* mice, in which two distinct GFP^{+}/tdT^{+} V1 subsets could be distinguished: a dorsal subset fully contained within the $V1^{Pou6f2}$ clade, and a ventral subset corresponding to $V1^{R}$ interneurons (Figure S5D). Approximately half of all $V1^{R}$ interneurons express MafA, and they serve as a proxy for the $V1^{MafA}$ clade (Figure S2E,F).

We found that $V1^{FoxP2}$, $V1^{Pou6f2}$, and $V1^{R}$ subsets could be distinguished by their passive and active membrane properties (Figure 4 and S5E-I). At hyperpolarized (< −80 mV) membrane potentials, distinctive active properties included: (i) the prominence of spike after-hyperpolarization (AHP) and early transient low-threshold depolarizations, (ii) the extent of initial spike bursting, and (iii) the degree of spike-frequency adaptation (SFA) during steady-state firing.

Analysis of $V1^{FoxP2}$ interneurons using whole-cell current-clamp recording revealed action potentials with a large and fast-rising AHP, no transient low-threshold depolarizations, no initial spike bursting, and little or no SFA (Figure 4A-C). $V1^{Pou6f2}$ interneurons segregated into a lateral bursting subset with a large low-threshold depolarization (Figure 4D, E) and a medial non-bursting subset with a much smaller transient depolarization (Figure 4G, H). At a molecular level these physiological distinctions likely correspond to the mediolateral positional segregation of $V1^{Pou6f2/Nr5a2}$ and $V1^{Pou6f2/Lmo3}$ interneurons (Figures 3E). Both $V1^{Pou6f2}$ subsets exhibited SFA, likely resulting from the buildup of long duration AHPs during successive spikes (Figure 4F, I). $V1^{R}$ interneurons exhibited a large low-threshold depolarization and short AHPs, resulting in a strong bursting phenotype with no evident SFA during steady state firing (Figure 4J-L). Thus, $V1^{FoxP2}$, $V1^{Pou6f2}$, and $V1^{R}$ interneurons can be distinguished by their biophysical properties, consistent with their molecular and positional segregation into distinct V1 clades.

Mapping the Relative Position of V1 Subpopulations and Motor Pools

The stereotypic nature of V1 neuronal position led us to examine whether the spinal motor system takes advantage of spatial segregation in the construction of inhibitory microcircuits. We focused on the connectivity of V1 subpopulations that settle at dorsal and ventral extremes of the parental V1 domain. Ventrally, we examined $V1^{R}$ interneurons, and as a dorsal comparator population we examined neurons in the $V1^{Sp8}$ clade (Figure 2E).

We employed intersectional and inducible genetic strategies to mark $V1^{Sp8}$ interneurons, generating a *Sp8::FlpoER*^{T2} transgenic mouse line and administering tamoxifen at p0, to evade the early expression of Sp8 in neuronal progenitors (Figure S6). The use of *Sp8::FlpoER*^{T2} and *En1::Cre* driver lines crossed to a *RCE.dual.GFP* reporter allele resulted in selective labeling of a cluster of $V1^{Sp8}$ interneurons in the dorsomedial region of the parental V1 domain (Figure 5A). To mark $V1^{R}$ interneurons we took advantage of their expression of calbindin (Figure 5B).

To probe the organizational features of inhibitory microcircuits that control limb musculature, we focused on three hindlimb motor pools. Gluteus (GL) motor neurons

innervate hip extensor muscles and occupy an extreme ventral position in the LMC. Tibialis anterior (TA) and instrinsic foot (IF) motor neurons innervate ankle flexor and foot plantar-flexor muscles respectively, and occupy a similar dorsal position within the LMC (McHanwell and Biscoe, 1981). Assessment of V1 subsets with respect to identified GL, TA, and IF motor pools in p21 *En1::Cre; Rosa.lsl.FP (tdT* or *eGFP)* mice indicated that $V1^{R}$ interneurons occupy a position close to that of GL motor neurons, whereas $V1^{Sp8}$ interneurons occupy a position close to that of TA and IF motor neurons (Figure 5C-E).

The dorsal and ventral positioning of the $V1^{R}$ and $V1^{Sp8}$ populations provided a spatial reference point for assessing three elements of spinal motor microcircuitry: (i) the nature of proprioceptive sensory input to V1 interneuron subsets, (ii) the nature of motor collateral input to V1 interneuron subsets and (iii) the organization of V1 interneuron output onto discrete motor neuron pools.

Positional Selectivity of Proprioceptive Sensory Inputs to $V1^{R}$ and $V1^{Sp8}$ Interneurons

We examined first whether $V1^{R}$ and $V1^{Sp8}$ interneurons receive sensory input, and if so, whether their settling position is predictive of proprioceptive input. Proprioceptive afferents target distinct D/V domains in a motor neuron-independent manner, as a function of their distal-to-proximal muscle origins in the limb (Sürmeli et al., 2011). On this basis we reasoned that the ventral restriction of $V1^{R}$ interneurons may constrain their ability to receive sensory input from dorsally-projecting proprioceptive afferents. In contrast, $V1^{Sp8}$ interneurons might receive input both from dorsally-projecting sensory afferents supplying more distal muscles, as well as from the collaterals of ventrally-projecting afferents supplying proximal musculature (Brown, 1981).

To determine the pattern of proprioceptive input to $V1^{R}$ and $V1^{Sp8}$ interneurons, we monitored the origin of proprioceptive terminals through transganglionic sensory transport and terminal accumulation of CTB after injection into individual limb muscles (Figure 6A,J). We found in ~p21 *En1::Cre; Rosa.lsl.tdT* mice that 47% (14/30) of $V1^{R}$ interneurons received input from CTB^{+}; $vGluT1^{+}$ GL sensory afferents. In contrast, only 5% (2/38) of $V1^{R}$ interneurons received input from TA afferents, and none (0/32) received input from IF afferents (Figure 6B,C). Differential innervation was not the result of preferential labeling of GL sensory afferents, in that we detected a similar incidence of homonymous CTB-labeled sensory terminals onto GL, TA, and IF motor neurons (Figure S7A,B).

To determine whether the profile of sensory contacts with $V1^{R}$ neurons correlates with functional input we monitored monosynaptic connections between proprioceptive afferents and $V1^{R}$ interneurons in an isolated spinal cord-hindlimb preparation (Figures 6D and S7E). In p4-p5 *En1::Cre; Rosa.lsl.tdT* mice, ventrally-positioned $tdTomato^{+}$ neurons were identified as $V1^{R}$ interneurons by virtue of their short-latency monosynaptic responses after antidromic stimulation of L4 or L5 ventral roots (Figure 6E). Individual muscle nerves were stimulated to activate defined classes of proprioceptive afferents. We found that 6 of 11 $V1^{R}$ interneurons responded to stimulation of the GL muscle nerve with EPSP latencies similar to those recorded from homonymous motor neurons (8.1 ± 0.3 ms and 8.4 ± 0.4 ms in $V1^{R}$ and motor neurons, respectively; Figure 6F,G). Moreover, repetitive stimulation of GL afferents at 0.1 or 1 Hz elicited EPSPs of low onset jitter in $V1^{R}$ interneurons ($CV_{onset} < 0.05$, Figures

6H,I and S7F), an indication of the monosynaptic nature of sensory input (Vrieseling and Arber, 2006).

TA and IF stimulation, in contrast, evoked long-latency input with variable onset to the vast majority of $V1^R$ interneurons, with only one TA neuron exhibiting a short latency, low jitter response (Figures 6F,H-I and S7F-H). Thus, physiological studies indicate selective input to $V1^R$ interneurons from proprioceptors innervating proximal (GL) muscles. Moreover, the strength of connections between GL proprioceptors and $V1^R$ interneurons indicates the existence of a selective group Ia-mediated feed-forward disynaptic inhibitory influence on motor output.

We next compared the pattern of proprioceptive sensory connections with $V1^{Sp8}$ interneurons. Analysis of ~p20 *En1::Cre; Sp8::FlpoER^{T2}; RCE.dual.GFP* mice revealed that ~15% of $V1^{Sp8}$ interneurons (7/44 cells) received CTB^+; $vGluT1^+$ contacts from GL afferents. TA sensory afferents formed synaptic contacts with ~40% of $V1^{Sp8}$ interneurons (23/58 cells) (Figure 6K,L; fraction of cells innervated by TA vs GL: $p = 0.004$ by Fisher's exact test). In addition, TA afferents established a >2-fold higher innervation density than GL afferents onto the proximal dendrites of $V1^{Sp8}$ interneurons. This increased incidence of TA connectivity suggests that dorsally-positioned $V1^{Sp8}$ interneurons receive a broader spectrum of proprioceptor input that ventrally-positioned $V1^R$ interneurons. In contrast, IF sensory afferents failed to contact $V1^{Sp8}$ interneurons (Figure 6K,L), an indication that proximity alone is not sufficient to explain all aspects of proprioceptive input to V1 interneurons. Despite the lack of IF sensory contacts, these findings support the idea that positional constraints imposed by the D/V matching of interneuron settling position and sensory afferent arborization domain explain many features of the pattern of selectivity of sensory input to $V1^R$ and $V1^{Sp8}$ interneurons.

Positional Constraints on V1 Interneuron-Motor Neuron Connections

We next considered whether the settling position of $V1^R$ and $V1^{Sp8}$ interneurons predicts their interconnectivity with motor neurons, analyzing first the extent to which $V1^R$ and $V1^{Sp8}$ interneurons receive motor neuron collateral input (Figure 7A). Analysis of the location of CTB^+; $vAChT^+$ motor axon collateral terminals indicated that GL and TA, but not IF motor axons form dense collateral arbors that are confined to a ventral domain overlapping with $V1^R$ interneurons, and ventral to $V1^{Sp8}$ interneurons (Figure S7D), in agreement with studies performed in cat (McCurdy and Hamm, 1992). By implication, $V1^R$ but not $V1^{Sp8}$ interneurons are positioned to receive synaptic input from GL and TA, but not IF, motor neurons.

To assess motor neuron input to $V1^R$ or $V1^{Sp8}$ interneurons, CTB was injected into individual muscles and motor axon collateral labeling analyzed in p21 *En1::Cre; RCE.lsl.GFP* or *En1::Cre*; *Sp8::FlpoER^{T2}; RCE.dual.GFP* tamoxifen-treated mice. The density of CTB-labeled, $vAChT^+$ boutons was determined on the soma and proximal dendrites of $V1^R$ and $V1^{Sp8}$ interneurons (Figure 7B-E). Both GL and TA motor neurons provide synaptic input to $V1^R$ interneurons, with each innervating about half of all $V1^R$ interneurons at comparable CTB^+; $vAChT^+$ bouton densities (Figure 7C). Nevertheless, $V1^R$ interneurons did not receive collateral input from IF motor neurons (Figure 7C). $V1^{Sp8}$

interneurons received no motor axon collateral contacts (Figure 7D,E), indicating that motor neuron collateral innervation is restricted to $V1^R$ interneurons, presumably a function of their ventral position. Thus, the settling position of $V1^R$ and $V1^{Sp8}$ interneurons predicts the status of motor as well as sensory neuron input.

We next examined whether subsets of V1 interneurons provide differential input to motor pools in accord with their settling position, focusing on the connections of $V1^R$ or $V1^{Sp8}$ interneurons with GL, TA, and IF motor neurons (Figure 7F). V1-derived, calbindin$^+$ terminals from $V1^R$ interneurons contacted GL and TA motor neurons at similar densities in ~p21 *En1::Cre; Rosa.lsl.tdT* or *En1::Cre; RCE.lsl.GFP* mice (Figure 7G,H; $p = 0.94$ or 0.84 for dendrites and soma, respectively, by two-tailed Student's t-test). Thus, ventrally located $V1^R$ interneurons target motor pools at different D/V locations with similar efficacy. In contrast, IF motor neurons received only sparse input from $V1^R$ neurons (Figure 7G,H), despite the similar D/V settling position of TA and IF motor pools (Figure 5C). The incidence of $V1^R$ innervation was ~7-fold greater on TA proximal dendrites and ~14-fold greater on TA soma, by comparison with IF motor neurons (Figure 7H). Thus the ventral position of $V1^R$ interneurons does not appear to constrain their ability to innervate motor neurons at different D/V positions, with the exception of a reduced innervation of the IF pool.

We also explored whether the dorsal settling position of $V1^{Sp8}$ interneurons limits their connectivity with motor neurons. In *En1::Cre*; *Sp8::FlpoER^{T2}; RCE.dual.GFP* mice, $V1^{Sp8}$ interneurons provided sparse and uniform contacts with GL, TA, and IF motor neurons (Figure 7I,J). The innervation density of $V1^{Sp8}$ inputs was <20% that of $V1^R$ inputs onto GL or TA motor neurons - although this value is likely to underestimate the actual incidence of motor neuron innervation, because only ~30% of $V1^{Sp8}$ interneurons are labeled after tamoxifen exposure (Figure S6E). These observations indicate that the dorsal position of $V1^{Sp8}$ interneurons does not limit their ability to innervate motor pools. Together, these data provide evidence that in spinal motor circuits the settling position of inhibitory interneurons is a determinant of input but not output connectivity.

DISCUSSION

Spinal interneurons shape motor activity and limb movement, but the organizational logic of their encoded microcircuits has remained obscure. Through a focus on V1 interneurons we identified nineteen transcription factors whose combinatorial expression documents extensive diversity within this inhibitory set. Different V1 subsets have distinct physiological characteristics and occupy stereotypic clustered positions in the ventral spinal cord, establishing a spatial plan with predictive relevance for inhibitory microcircuit organization. Indeed, variant V1 microcircuits are used to control motor pools that innervate muscles at different limb joints, documenting the absence of a fixed circuit architecture for interneurons that control limb movement (Figure 7K).

Interneuron Diversity and its Implications for Motor Control

V1 interneurons comprise a highly diverse set of transcriptionally distinct neuronal types, posing questions about the purpose of such heterogeneity. We have found that the

transcriptional diversity of V1 clades matches physiologically distinct excitable properties. Diversity may also reflect the demand that interneurons receive varied inputs from numerous sources. The activity of motor neurons is regulated by over a dozen supraspinal neuronal systems (Lemon, 2008), many of which engage only a restricted set of all possible motor pools: thus rubrospinal input is restricted to motor pools controlling distal muscles, and vestibulospinal input to motor pools innervating extensor muscles (Grillner and Hongo, 1972; McCurdy et al., 1987). These descending systems presumably engage interneurons with a selectivity that matches the specificity of motor neuron recruitment. Distinct subsets of V1 interneurons may therefore be recruited by different descending systems so as to link sensory input with intermediary descending control pathways. The high degree of V1 transcriptional diversity could provide a means of establishing distinctions in settling position or molecular recognition cues that facilitate the integration of multiple input systems and output modules.

The heterogeneity exhibited by V1 interneurons is likely to extend to other spinal interneuron populations. Small subsets of spinal V0 interneurons have been delineated on the basis of selective profiles of transcription factor expression, best exemplified by a compact cluster of $Pitx2^{+}$ $V0_{C}$ interneurons that represent the source of cholinergic C-bouton inputs to motor neurons (Zagoraiou et al., 2009). Moreover, many of the transcription factors that delineate V1 subsets are expressed by small subsets of inhibitory V2b and excitatory V2a interneurons, raising the possibility that conserved elements of input and output wiring specificity are encoded by a common set of transcription factors within different excitatory and inhibitory interneuron sets. If the extent of diversity of V1 interneurons extends to each cardinal (V0, V2a/b, and V3) interneuron population (Francius et al., 2013), the fidelity of motor output could depend on the coordinated activity of > 200 subsets of ventral interneurons.

It remains unclear whether the diversity evident in V1 interneurons has predictive relevance for other CNS circuits. The spinal motor system could require a greater degree of interneuron diversification than the brain, because of the last-order and non-redundant nature of motor neuron output and the behavioral imperative to confer precise patterns of muscle activation. Nevertheless, the predictive view may be nearer the mark. Single-cell transcriptional profiling from interneurons in primary somatosensory cortex and CA1 hippocampus have revealed at least sixteen different subsets, with the potential for yet greater diversity (Zeisel et al., 2015). In addition, many of the transcription factors that delineate subsets of V1 interneurons are expressed by subsets of cortical interneurons (Tasic et al., 2016). Thus, it is likely that principles of spinal interneuron heterogeneity and function have relevance for circuit organization and function in the brain.

Position as a Determinant in the Organization of Inhibitory Microcircuits

The relevance of neuronal settling position in spinal connectivity has emerged from studies on the synaptic organization of sensory connections with motor neurons. Proprioceptive afferents target distinct dorsoventral domains of the ventral spinal cord in a manner independent of motor neuron character (Sürmeli et al., 2011), and thus the stereotypy of settling position is needed for the formation of selective sensory connections. Similarly, $V1^{R}$

interneurons receive input from ventrally projecting hip afferents, whereas dorsal $V1^{Sp8}$ interneurons receive input both from dorsally-directed ankle afferents as well as from hip afferents. Thus, V1 positional stereotypy has implications for motor microcircuit organization in the realm of input selectivity.

The finding that $V1^{R}$ interneurons receive selective input from hip muscle afferents sheds light on a long-standing uncertainty about the status of sensory input to $V1^{R}$ interneurons. Classical studies in cat focused on sensory feedback from knee and ankle muscles, and argued for the absence of functional monosynaptic sensory connectivity with $V1^{R}$ interneurons (Ryall and Piercey, 1971). Later studies in rodent spinal cord, however, provided physiological evidence for direct sensory input to $V1^{R}$ interneurons during early postnatal development (Mentis et al., 2006). These divergent conclusions can be reconciled through an appreciation of the dominance of proprioceptive input from hip afferents, an afferent source not examined in cat. Nevertheless, the extent to which this circuit functions at later developmental stages is unclear because the strength of sensory inputs to $V1^{R}$ interneurons decreases in the adult (Mentis et al., 2006).

The density of hip afferent inputs to $V1^{R}$ interneurons presumably forms a disynaptic feedforward inhibitory pathway to motor neurons, in addition to the role of $V1^{R}$ interneurons in recurrent inhibition. Sensory-evoked feedforward inhibition could modulate the temporal features and dynamic range of excitatory responses of hip motor neurons, as with inhibitory interneurons in hippocampal and cortical circuits (Pouille et al., 2009). An inhibitory signal dependent on hip position could also modulate flexion/extension transitions during the step cycle (McVea et al., 2005) and/or reflex actions at the ankle joint (Knikou and Rymer, 2002).

The link between interneuron settling position and microcircuit wiring is so far largely correlative. Nevertheless our data, combined with previous findings on the relevance of motor neuron positioning (Sürmeli et al., 2011), supports the view that the precision of interneuron location constrains circuit wiring. The role of neuronal settling position in organizing interneuron circuits appears restricted to input connectivity. V1 interneuron position is not predictive of motor pool target connections, reminiscent of observations that motor neuron settling position is not required for the innervation of specific limb muscles (Demireva et al., 2011).

Positional constraints are likely to act in conjunction with molecular recognition systems in defining final connectivity profiles. Precedent for such recognition systems has emerged from analysis of repellant sema3e-plexinD1 signaling in sensory-motor connectivity (Fukuhara et al., 2013; Pecho-Vrieseling et al., 2009). The existence of repellent cues could explain how the dorsal termination zone of IF sensory afferents is not associated with direct synaptic contact with $V1^{Sp8}$ interneurons, despite the proximity of presynaptic axons and $V1^{Sp8}$ dendrites. In addition, the extent of interneuron dendritic arborization could relieve constraints on input connectivity imposed by somatic clustering. Although the dendritic arbors of $V1^{R}$ interneurons are largely confined to the ventral spinal cord (Lagerback and Kellerth, 1985), $V1^{Sp8}$ interneurons exhibit larger dendritic arbors (J. Bikoff, unpublished

observation), potentially expanding synaptic input. Thus it seems unlikely that position alone directs input connectivity with V1 subsets.

Variant Microcircuits for Joints and Muscles

The variant circuit architectures exhibited by V1 interneurons may be a general feature of spinal motor microcircuits. The anatomical and physiological characterization of the circuitry of $V1^R$ interneurons is consistent with physiological descriptions in cat of a reduced degree of recurrent inhibition for motor neurons that innervate distal compared to proximal limb musculature (Illert and Wietelmann, 1989; McCurdy and Hamm, 1992). Thus, recurrent inhibition is not implemented uniformly across motor pools. Other classically-defined inhibitory motifs also exhibit variant circuit architecture: Group Ib feedforward inhibition is strongly activated by extensor afferents, but only weakly by flexor afferents (Eccles et al., 1957). Moreover, reciprocal inhibition is prominent for flexor/extensor antagonist pairs, but absent for abductor/adductor antagonists (Eccles and Lundberg, 1958). Local motor microcircuits are therefore differentially tailored to the workings of individual muscles.

Finally, our studies raise the issue of the functional consequences of variation in V1 interneuron microcircuitry. Evolutionary adaptation for dexterous hand movements has fine-tuned the ability of distal limb muscles to control digits independently. Yet recurrent inhibition functions broadly to silence motor pools (Eccles et al., 1961), suggesting that the absence of recurrent inhibition in distal musculature contributes to the independence of neural control for individual digit muscles. From an evolutionary perspective, the diversity exhibited by mammalian V1 interneuron circuits may be needed to accommodate the complex control features of multi-joint limbs.

EXPERIMENTAL PROCEDURES

Mouse Genetics

Mouse lines are described in Supplemental Experimental Procedures. All experiments and procedures were performed according to NIH guidelines and approved by the Institutional Animal Care and Use Committee of Columbia University.

Microarray Screen

Fluorescence activated cell sorting, RNA processing, and microarray analyses are described in Supplemental Experimental Procedures. Microarray data are available at the NCBI Gene Expression Omnibus, under accession number GSE69560.

Immunohistochemistry

Immunohistochemistry was performed as described (Betley et al., 2009). Confocal images of cryostat or vibratome-sectioned tissue were obtained on a LSM 710 Meta Confocal microscope (Carl Zeiss). Antibodies, immunohistochemical methods, and detection of transcription factor co-expression are documented in Supplemental Experimental Procedures.

Analysis of Interneuron Spatial Distributions

V1 interneuron positional analysis is described in Supplemental Experimental Procedures.

Retrograde Labeling of Motor and Sensory Neurons

Motor and sensory neurons were retrogradely labeled *in vivo* at p14-p16 by intramuscular injection of 1% unconjugated cholera toxin B subunit (CTB, List Biologicals). Animals were analyzed after 5-7 days (Sürmeli et al., 2011). Details are described in Supplemental Experimental Procedures.

Synaptic Quantification

Synaptic quantification is presented in Supplemental Experimental Procedures.

Electrophysiology

Recordings from intact spinal cord-hindlimb preparations were performed as described (Mentis et al., 2005), with connectivity to GL, TA, and IF peripheral muscles preserved. Recordings from V1 subsets were obtained in 300 μm thick slices as described (Gonzalez-Forero and Alvarez, 2005). Details are provided in Supplemental Experimental Procedures.

Statistics

Significance between means was assessed with an unpaired two-tailed Student's t-test, or a one-way ANOVA and Bonferroni *post-hoc* test. Fisher's exact test was used to compare the proportion of neurons receiving synaptic input from different muscles. All data are represented as mean ± SEM unless noted. Statistical methods for spatial distributions are presented in Supplemental Experimental Procedures.

Supplementary Material

Refer to Web version on PubMed Central for supplementary material.

ACKNOWLEDGEMENTS

We are grateful to I. Schieren for help with FACS, B. Han and M. Mendelsohn for help generating transgenic mice, and K. MacArthur for manuscript preparation. We thank A. Joyner for advice on generating FlpoER^{T2}, G. Fishell for *RCE.dual.GFP* mice, and K. Campbell for *Sp8$^{fl/fl}$* mice. J. Nathans provided anti-Nr3b2, and S. Ross anti-Bhlhb5 and anti-Prdm8 antibodies. We thank R. Axel, E. Azim, N. Balaskas, R. Brownstone, and J. de Nooij for discussions and comments on the manuscript. F.J.A. was supported by NIH-NINDS (R01-NS047357.) G.Z.M. was supported by the NIH (R01-NS078375 and R21-NS079981) and the Department of Defense (GR.10235006). T.M.J was supported by NIH grant NS033245, the Brain Research Foundation, the Harold and Leila Y. Mathers Foundation and Project A.L.S., and is an HHMI investigator.

REFERENCES

Alvarez FJ, Fyffe REW. The continuing case for the Renshaw cell. J. Physiol. 2007; 584:31–45. [PubMed: 17640932]

Arber S. Motor circuits in action: specification, connectivity, and function. Neuron. 2012; 74:975–989. [PubMed: 22726829]

Baldissera F, Hultborn H, Illert M. Brooks VB. Integration in spinal neuronal systems. Handbook of Physiology, The Nervous System. 1981:509–595.

Benito-Gonzalez A, Alvarez FJ. Renshaw cells and Ia inhibitory interneurons are generated at different times from p1 progenitors and differentiate shortly after exiting the cell cycle. J. Neurosci. 2012; 32:1156–1170. [PubMed: 22279202]

Betley JN, Wright CV, Kawaguchi Y, Erdelyi F, Szabo G, Jessell TM, Kaltschmidt JA. Stringent specificity in the construction of a GABAergic presynaptic inhibitory circuit. Cell. 2009; 139:161–174. [PubMed: 19804761]

Briscoe J, Pierani A, Jessell TM, Ericson J. A homeodomain protein code specifies progenitor cell identity and neuronal fate in the ventral neural tube. Cell. 2000; 101:435–445. [PubMed: 10830170]

Brown, AG. Organization in the Spinal Cord: The Anatomy and Physiology of Identified Neurones. Springer-Verlag; New York: 1981.

Dalla Torre di Sanguinetto SA, Dasen JS, Arber S. Transcriptional mechanisms controlling motor neuron diversity and connectivity. Curr. Opin. Neurobiol. 2008; 18:36–43. [PubMed: 18524570]

Demireva EY, Shapiro LS, Jessell TM, Zampieri N. Motor neuron position and topographic order imposed by β- and γ-catenin activities. Cell. 2011; 147:641–652. [PubMed: 22036570]

Eccles JC, Eccles RM, Iggo A, Ito M. Distribution of recurrent inhibition among motoneurones. J. Physiol. 1961; 159:479–499. [PubMed: 13889048]

Eccles JC, Eccles RM, Lundberg A. Synaptic actions on motoneurones caused by impulses in Golgi tendon organ afferents. J. Physiol. 1957; 138:227–252. [PubMed: 13526123]

Eccles RM, Lundberg A. Integrative pattern of Ia synaptic actions on motoneurones of hip and knee muscles. J. Physiol. 1958; 144:271–298. [PubMed: 13611693]

Francius C, Harris A, Rucchin V, Hendricks TJ, Stam FJ, Barber M, Kurek D, Grosveld FG, Pierani A, Goulding M, et al. Identification of multiple subsets of ventral interneurons and differential distribution along the rostrocaudal axis of the developing spinal cord. PLoS ONE. 2013; 8:e70325. [PubMed: 23967072]

Fukuhara K, Imai F, Ladle DR, Katayama K, Leslie JR, Arber S, Jessell TM, Yoshida Y. Specificity of monosynaptic sensory-motor connections imposed by repellent Sema3E-PlexinD1 signaling. Cell Rep. 2013; 5:748–758. [PubMed: 24210822]

Fyffe RE. Evidence for separate morphological classes of Renshaw cells in the cat's spinal cord. Brain Res. 1990; 536:301–304. [PubMed: 2085756]

Gabitto MI, Pakman A, Bikoff JB, Abbott LF, Jessell TM, Paninski L. Bayesian sparse regression analysis documents the diversity of spinal inhibitory interneurons. Cell. 2016 this issue.

Glasgow SM, Henke RM, Macdonald RJ, Wright CV, Johnson JE. Ptf1a determines GABAergic over glutamatergic neuronal cell fate in the spinal cord dorsal horn. Development. 2005; 132:5461–5469. [PubMed: 16291784]

Gonzalez-Forero D, Alvarez FJ. Differential postnatal maturation of GABAA, glycine receptor, and mixed synaptic currents in Renshaw cells and ventral spinal interneurons. J. Neurosci. 2005; 25:2010–2023. [PubMed: 15728841]

Gosgnach S, Lanuza GM, Butt SJ, Saueressig H, Zhang Y, Velasquez T, Riethmacher D, Callaway EM, Kiehn O, Goulding M. V1 spinal neurons regulate the speed of vertebrate locomotor outputs. Nature. 2006; 440:215–219. [PubMed: 16525473]

Goulding M, Bourane S, Garcia-Campmany L, Dalet A, Koch S. Inhibition downunder: an update from the spinal cord. Curr. Opin. Neurobiol. 2014; 26:161–166. [PubMed: 24743058]

Grillner S, Hongo T. Vestibulospinal effects on motoneurones and interneurones in the lumbosacral cord. Prog. Brain Res. 1972; 37:243–262. [PubMed: 4642044]

Hultborn H, Jankowska E, Lindstrom S. Recurrent inhibition of interneurones monosynaptically activated from group Ia afferents. J. Physiol. 1971; 215:613–636. [PubMed: 4253675]

Illert M, Wietelmann D. Distribution of recurrent inhibition in the cat forelimb. Prog. Brain Res. 1989; 80:273–281. [PubMed: 2699367]

Jankowska E. Interneuronal relay in spinal pathways from proprioceptors. Prog. Neurobiol. 1992; 38:335–378. [PubMed: 1315446]

Knikou M, Rymer Z. Effects of changes in hip joint angle on H-reflex excitability in humans. Exp. Brain Res. 2002; 143:149–159. [PubMed: 11880891]

Lagerback PA, Kellerth JO. Light microscopic observations on cat Renshaw cells after intracellular staining with horseradish peroxidase. II. The cell bodies and dendrites. J. Comp. Neurol. 1985; 240:368–376. [PubMed: 3880356]

Lemon RN. Descending pathways in motor control. Annu. Rev. Neurosci. 2008; 31:195–218. [PubMed: 18558853]

Matise MP, Joyner AL. Expression patterns of developmental control genes in normal and Engrailed-1 mutant mouse spinal cord reveal early diversity in developing interneurons. J. Neurosci. 1997; 17:7805–7816. [PubMed: 9315901]

McCurdy ML, Hansma DI, Houk JC, Gibson AR. Selective projections from the cat red nucleus to digit motor neurons. J. Comp. Neurol. 1987; 265:367–379. [PubMed: 2447133]

McCurdy ML, Hamm TM. Recurrent collaterals of motoneurons projecting to distal muscles in the cat hindlimb. J. Neurophysiol. 1992; 67:1359–1366. [PubMed: 1597718]

McHanwell S, Biscoe TJ. The localization of motoneurons supplying the hindlimb muscles of the mouse. Philos. Trans. R. Soc. of Lond. B, Biol. Sci. 1981; 293:477–508. [PubMed: 6115428]

McVea DA, Donelan JM, Tachibana A, Pearson KG. A role for hip position in initiating the swing-to-stance transition in walking cats. J. Neurophysiol. 2005; 94:3497–3508. [PubMed: 16093331]

Mentis GZ, Alvarez FJ, Bonnot A, Richards DS, Gonzalez-Forero D, Zerda R, Donovan MJ. Noncholinergic excitatory actions of motoneurons in the neonatal mammalian spinal cord. Proc. Natl. Acad. Sci. USA. 2005; 102:7344–7349. [PubMed: 15883359]

Mentis GZ, Siembab VC, Zerda R, O'Donovan MJ, Alvarez FJ. Primary afferent synapses on developing and adult Renshaw cells. J. Neurosci. 2006; 26:13297–13310. [PubMed: 17182780]

Pecho-Vrieseling E, Sigrist M, Yoshida Y, Jessell TM, Arber S. Specificity of sensory-motor connections encoded by Sema3e-Plxnd1 recognition. Nature. 2009; 459:842–846. [PubMed: 19421194]

Pouille F, Marin-Burgin A, Adesnik H, Atallah BV, Scanziani M. Input normalization by global feedforward inhibition expands cortical dynamic range. Nat. Neurosci. 2009; 12:1577–1585. [PubMed: 19881502]

Ryall RW, Piercey MF. Excitation and inhibition of Renshaw cells by impulses in peripheral afferent nerve fibers. J. Neurophysiol. 1971; 34:242–251. [PubMed: 4251020]

Sanes JR, Masland RH. The Types of Retinal Ganglion Cells: Current Status and Implications for Neuronal Classification. Annu. Rev. Neurosci. 2015; 38:221–246. [PubMed: 25897874]

Sapir T, Geiman EJ, Wang Z, Velasquez T, Mitsui S, Yoshihara Y, Frank E, Alvarez FJ, Goulding M. Pax6 and Engrailed1 regulate two distinct aspects of Renshaw cell development. J. Neurosci. 2004; 24:1255–1264. [PubMed: 14762144]

Saueressig H, Burrill J, Goulding M. Engrailed-1 and Netrin-1 regulate axon pathfinding by association interneurons that project to motor neurons. Development. 1999; 126:4201–4212. [PubMed: 10477289]

Stam FJ, Hendricks TJ, Zhang J, Geiman EJ, Francius C, Labosky PA, Clotman F, Goulding M. Renshaw cell interneuron specialization is controlled by a temporally restricted transcription factor program. Development. 2012; 139:179–190. [PubMed: 22115757]

Sürmeli G, Akay T, Ippolito GC, Tucker PW, Jessell TM. Patterns of spinal sensory-motor connectivity prescribed by a dorsoventral positional template. Cell. 2011; 147:653–665. [PubMed: 22036571]

Tasic B, Menon V, Nguyen TN, Kim TK, Jarsky T, Yao Z, Levi B, Gray LT, Sorensen SA, Dolbeare T, et al. Adult mouse cortical cell taxonomy revealed by single cell transcriptomics. Nat. Neurosci. 2016 doi:10.1038/nn.4216.

Vrieseling E, Arber S. Target-induced transcriptional control of dendritic patterning and connectivity in motor neurons by the ETS gene Pea3. Cell. 2006; 127:1439–1452. [PubMed: 17190606]

Windhorst U. Muscle proprioceptive feedback and spinal networks. Brain Res. Bull. 2007; 73:155–202. [PubMed: 17562384]

Zagoraiou L, Akay T, Martin JF, Brownstone RM, Jessell TM, Miles GB. A cluster of cholinergic premotor interneurons modulates mouse locomotor activity. Neuron. 2009; 64:645–662. [PubMed: 20005822]

Zeisel A, Munoz-Manchado AB, Codeluppi S, Lonnerberg P, La Manno G, Jureus A, Marques S, Munguba H, He L, Betsholtz C, et al. Cell types in the mouse cortex and hippocampus revealed by single-cell RNA-seq. Science. 2015; 347:1138–1142. [PubMed: 25700174]

Zhang Y, Lupton R, Lanuza GM, Britz O, Wang Z, Siembab VC, Velasquez T, Alvarez FJ, Frank E, Goulding M. V1 and V2b interneurons secure the alternating flexor-extensor motor activity mice require for limbed locomotion. Neuron. 2014; 82:138–150. [PubMed: 24698273]

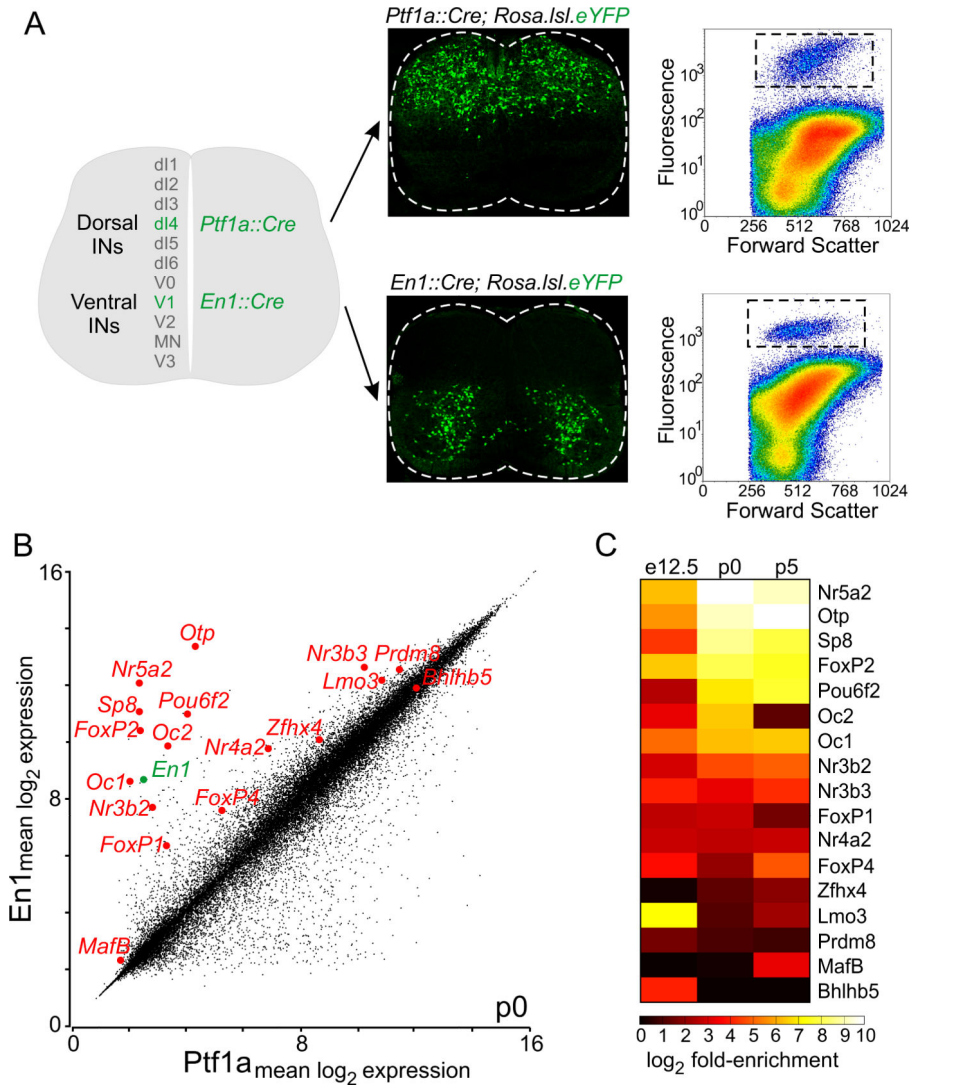

Figure 1. Transcription Factors Enriched in V1 Interneurons

(A) Isolation of V1 and dI4/dIL^{A} interneurons. Left, interneuron populations. Middle, *En1::Cre* (V1) and *Ptf1a::Cre* (dI4/dIL^{A}) lineage-traced interneurons in p0 lumbar spinal cord. Right, FACS-isolated eYFP^{+} interneurons for microarray analysis.

(B) Scatter plot of expression levels of transcription factors (TFs, red) enriched in V1 interneurons from p0 mice.

(C) TFs with > 3-fold enrichment ($p \leq 0.02$, one-way ANOVA) at one or more developmental ages. See also Figure S1.

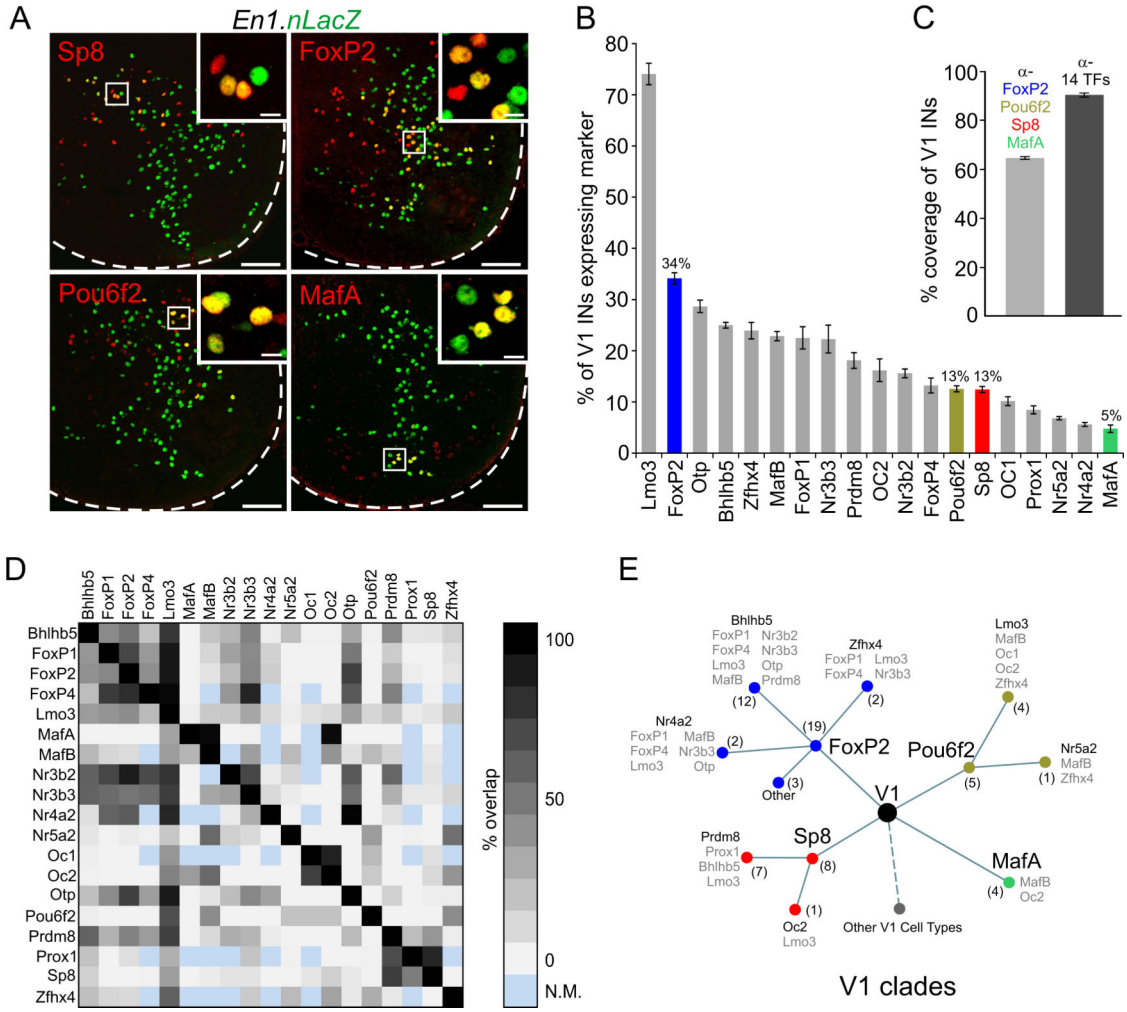

Figure 2. V1 Transcriptional Diversity and Cladistic Analysis

(A) TFs (red) label subsets of V1 interneurons (green) in L3-L5 spinal segments from p0 *En1.nLacZ* mice. Scale bars = 100 μm or 10 μm (inset).

(B) V1 interneurons expressing TFs at p0 L3-L5 spinal segments (n ≥ 3 animals, mean ± SEM). See Figure S2B,C for characterization of TFs in dI4/dIL^{A} and V2a interneurons.

(C) Coverage of V1 interneurons in p0 L3-L5 spinal cord. Anti-FoxP2, MafA, Pou6f2, and Sp8 antibodies label 64.2 ± 0.6% of V1 interneurons (n = 3). Application of 14 antibodies - Bhlhb5, FoxP1, FoxP2, MafB, Nr3b2, Nr4a2, Nr5a2, Oc1, Oc2, Otp, Pou6f2, Prdm8, Prox1, and Sp8 - labels 90.4 ± 0.8% of V1 interneurons (n = 3). Mean ± SEM.

(D) Matrix of pairwise overlap for 148 out of 171 comparisons. N.M. = not measured, due to antibody incompatibility.

(E) V1 interneurons segregate into four clades defined by mutually exclusive expression of FoxP2, MafA, Pou6f2, and Sp8 (< 1% overlap in each pairwise comparison). Clades are further subdivided by distinct TFs (black). Dotted line represents additional V1 cell types. The number of V1 cell types is indicated in parenthesis. See also Figures S2D and S3C.

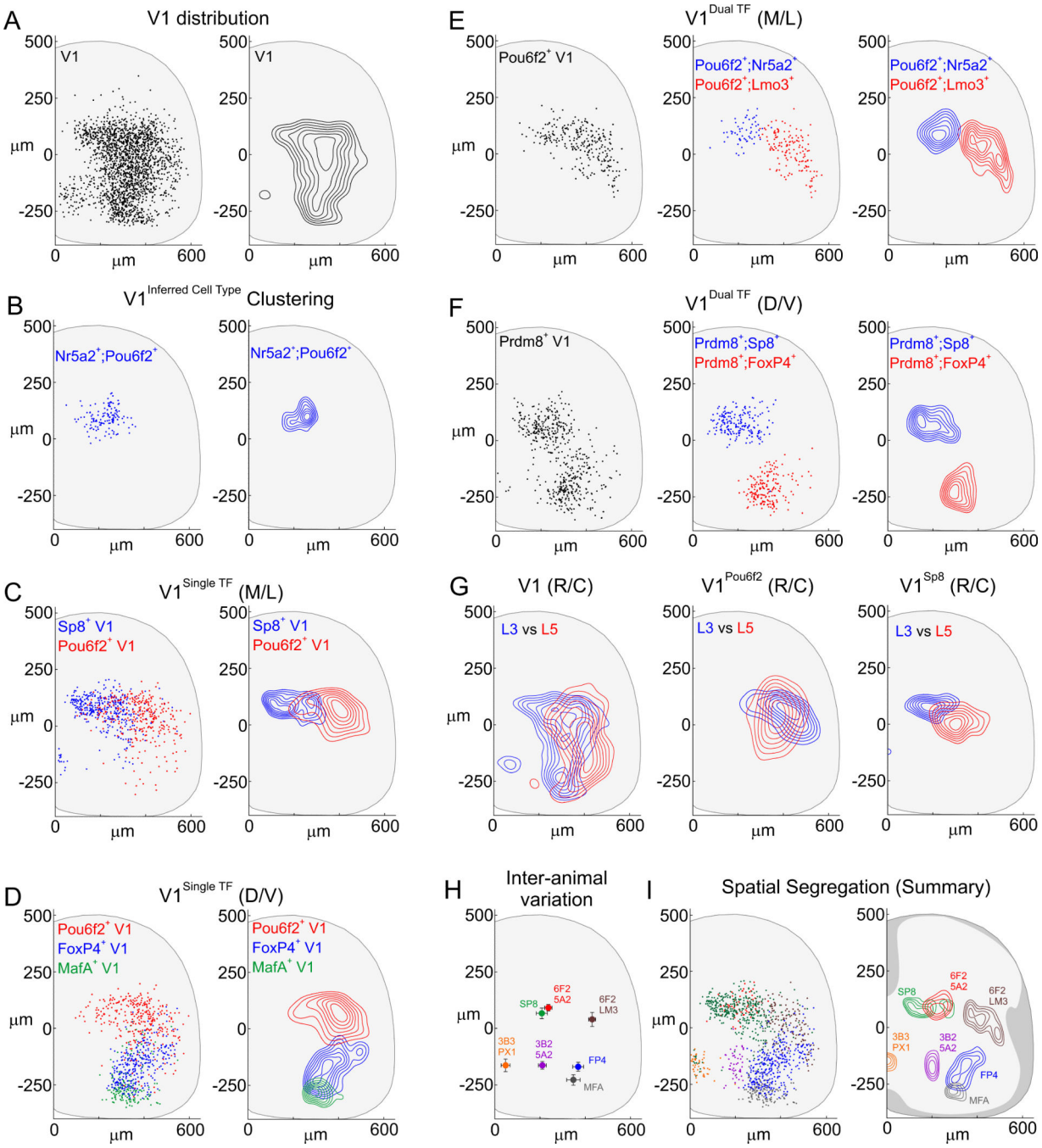

Figure 3. Spatial Segregation of V1 Interneuron Subpopulations

(A) V1 interneurons in p0 L3-L5 segments of *En1.nLacZ* mice. D/V axis range: 132 to −265 μm; M/L axis range: 127 to 487 μm, 5th-95th percentiles from central canal. Contours represent density at the 30th-90th percentiles.

(B) Spatial clustering of V1$^{Pou6f2/Nr5a2}$ interneurons (blue, F_a = 0.236) ($p < 0.00001$, one-tailed Monte Carlo test compared to parental V1).

(C) M/L biases in distributions of $V1^{Sp8}$ ($X_{epicenter}$ = 162 μm) and $V1^{Pou6f2}$ (X_{epi} = 403 μm) interneurons. $p < 1 \times 10^{-20}$, Wilcoxon Rank Sum test in x-axis, $V1^{Sp8}$ or $V1^{Pou6f2}$ vs $V1^{Parental}$, and $V1^{Sp8}$ vs $V1^{Pou6f2}$.

(D) D/V biases in distributions of $V1^{Pou6f2}$ (Y_{epi} = 66 μm), $V1^{FoxP4}$ (Y_{epi} = −158 μm), and $V1^{MafA}$ (Y_{epi} = −277 μm) interneurons. $V1^{Sp8}$ interneurons (Y_{epi} = 72 μm) also occupy a dorsal position. $p < 1 \times 10^{-20}$, Wilcoxon Rank Sum test in y-axis for $V1^{Pou6f2}$, $V1^{FoxP4}$, $V1^{MafA}$, or $V1^{Sp8}$ vs $V1^{Parental}$.

E) Subdivision of $V1^{Pou6f2}$ interneurons into medial ($Nr5a2^+$, blue) and lateral ($Lmo3^+$, red) subsets in p0 L3-L4 spinal segments.

(F) $V1^{Prdm8}$ interneurons fractionate into dorsal $Sp8^+$ (blue) and ventral $FoxP4^+$ (red) composite groups.

(G) V1, $V1^{Pou6f2}$, and $V1^{Sp8}$ settling position at L3 (blue) or L5 (red) in p0 mice. $p < 0.0001$ for L3 vs L5, 2D KS test.

(H) Constancy of x,y position (mean ± SD) for V1 interneurons expressing Sp8 (n = 7), Pou6f2/Nr5a2 (n = 8), Pou6f2/Lmo3 (n = 4), FoxP4 (n = 7), Nr3b2/Nr5a2 (n = 8), Nr3b3/Prox1 (n = 6), and MafA (n = 7 animals).

(I) Spatial distributions of seven V1 subsets. Contours represent 60^{th}-90^{th} percentile densities. See also Figures S3 and S4, and Table S1.

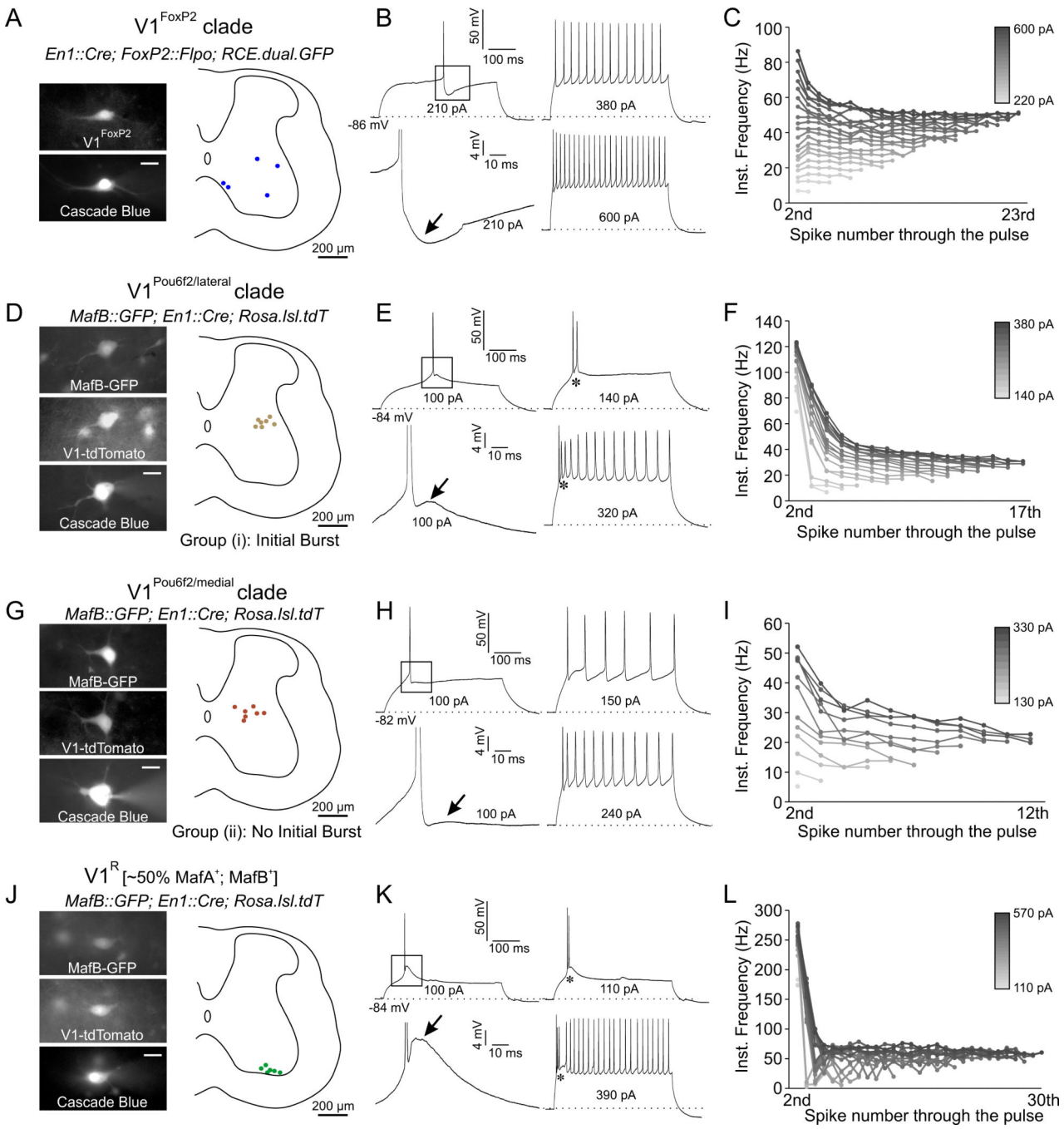

Figure 4. Electrophysiological Characterization of V1 Clades

(A-C) Physiology of $V1^{FoxP2}$ interneurons. (A) $V1^{FoxP2}$ interneurons (n = 5) targeted for recording and filled with Cascade Blue in *En1::Cre; FoxP2::Flpo; RCE.dual.GFP* mice. Scale bar = 20 μm. (B) Firing properties of $V1^{FoxP2}$ cells show a prominent after-hyperpolarization (AHP, arrow), a non-bursting phenotype, and an absence of spike frequency adaptation (SFA). (C) Instantaneous firing (IF) frequency for each action potential (dot) through pulses of increasing current amplitudes (20 pA steps). Little or no SFA is observed below 460 pA.

(D-F) Physiology of $V1^{Pou6f2/lateral}$ interneurons. (D) Position of $V1^{Pou6f2/lateral}$ interneurons (n = 7) in *MafB::GFP; En1::Cre; Rosa.lsl.tdT* mice. (E) Transient low-threshold depolarization (arrow), with an initial burst (asterisks), and the presence of SFA throughout the pulse. (F) SFA, indicated by the decreasing instantaneous frequency of successive action potentials.

(G-I) Physiology of $V1^{Pou6f2/medial}$ interneurons. (G) Position of $V1^{Pou6f2/medial}$ interneurons (n = 7). (H) Neurons exhibit a non-burst phenotype and a weak low-threshold depolarization (arrow, H). (I) IF plot showing SFA.

(J-L) Physiology of $V1^{R}$ interneurons, representing the $V1^{MafA}$ clade. (J) Position of $V1^{R}$ interneurons (n = 6) in *En1::Cre; Rosa.lsl.tdT; MafB::GFP* mice. (K) Neurons show prominent low-threshold depolarization (arrow), and burst firing (asterisks). (L) IF plot shows absence of SFA. See also Figure S5.

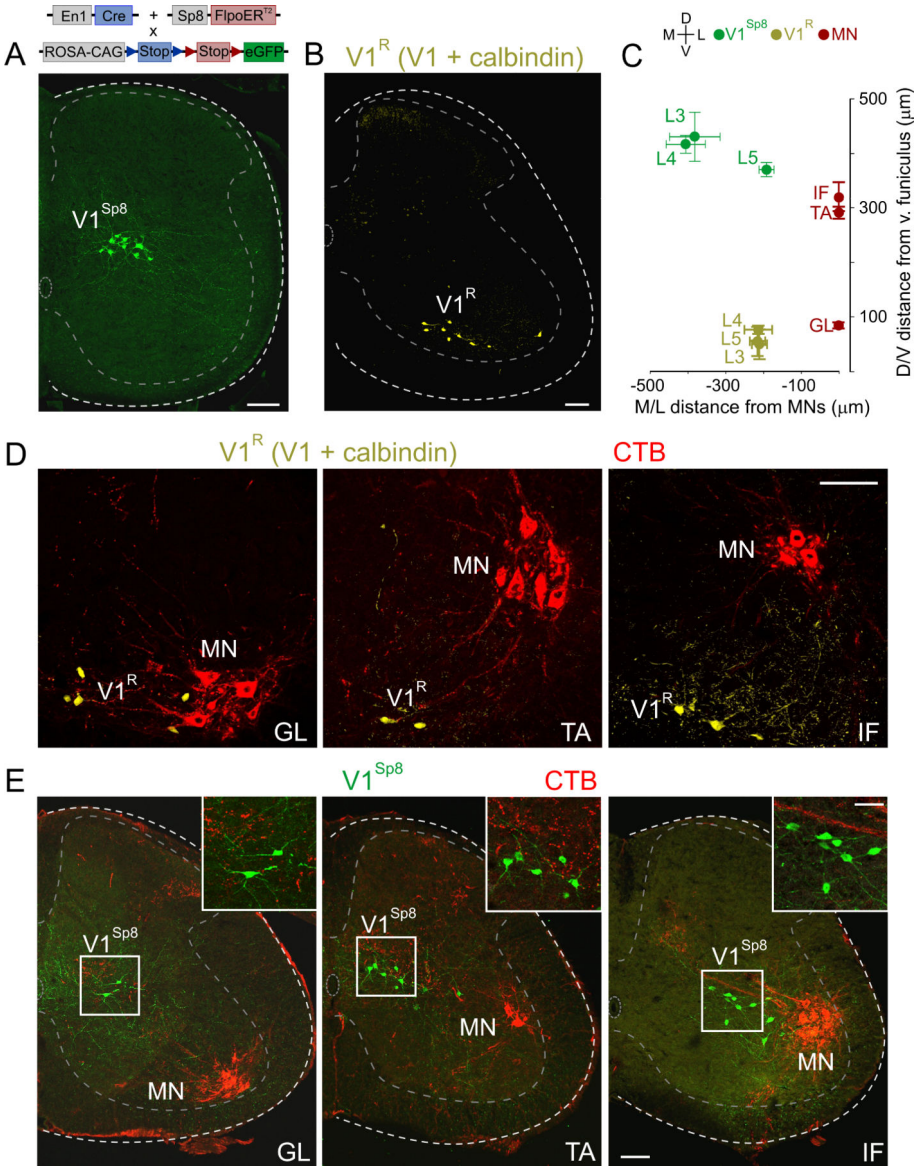

Figure 5. Relative Position of V1^{R} and V1^{Sp8} Interneurons to Motor Pools

(A) V1^{Sp8} interneurons (green), in p12 lumbar spinal cord of *En1::Cre; Sp8::FlpoER^{T2}; RCE.dual.GFP* mice.

(B) V1^{R} interneurons (yellow, colocalization mask of eGFP and calbindin immunoreactivity) in ~p21 *En1::Cre; RCE.lsl.GFP* lumbar spinal cord.

(C) V1^{R} and V1^{Sp8} position with respect to GL, TA, and IF motor pools in ~p21 mice. Motor pool D/V positions: GL: 84 ± 3 μm, TA: 291 ± 6 μm, IF: 321 ± 15 μm, from dorsal border of ventral funiculus.

(D) D/V position of V1^{R} interneurons (yellow) with respect to CTB-backfilled GL, TA, and IF motor pools (MN, red) in ~p21 lumbar spinal cord. D/V distances: V1^{R} ventral to GL, TA, and IF motor neurons by 8 ± 3 μm, 242 ± 14 μm, and 264 ± 13 μm, respectively. $p < 0.0001$, one-way ANOVA; Bonferroni *post-hoc* test: $p < 0.001$, TA or IF vs GL. M/L distances were not significantly different ($p = 0.99$, one-way ANOVA).

(E) D/V position of $V1^{Sp8}$ interneurons (green) with respect to CTB-backfilled GL, TA, and IF motor pools (red) in ~p21 lumbar spinal cord. $V1^{Sp8}$ dorsal to GL, TA, and IF by 332 ± 8 μm, 139 ± 23 μm, and 50 ± 8 μm, respectively ($p < 0.0001$, one-way ANOVA; Bonferroni *post-hoc* test: $p < 0.001$, TA or IF vs GL; $p < 0.05$, TA vs IF). In the M/L axis, $V1^{Sp8}$ interneurons were significantly closer to IF than to GL or TA (192 ± 11 μm versus 406 ± 26 μm or 382 ± 33 μm, respectively; $p < 0.01$, one-way ANOVA; Bonferroni *post-hoc* test; $p < 0.01$, IF vs GL or TA). Values are mean ± SEM, $n \geq 3$ animals per condition. Scale bars = 100 μm or 50 μm (inset). See also Figure S6.

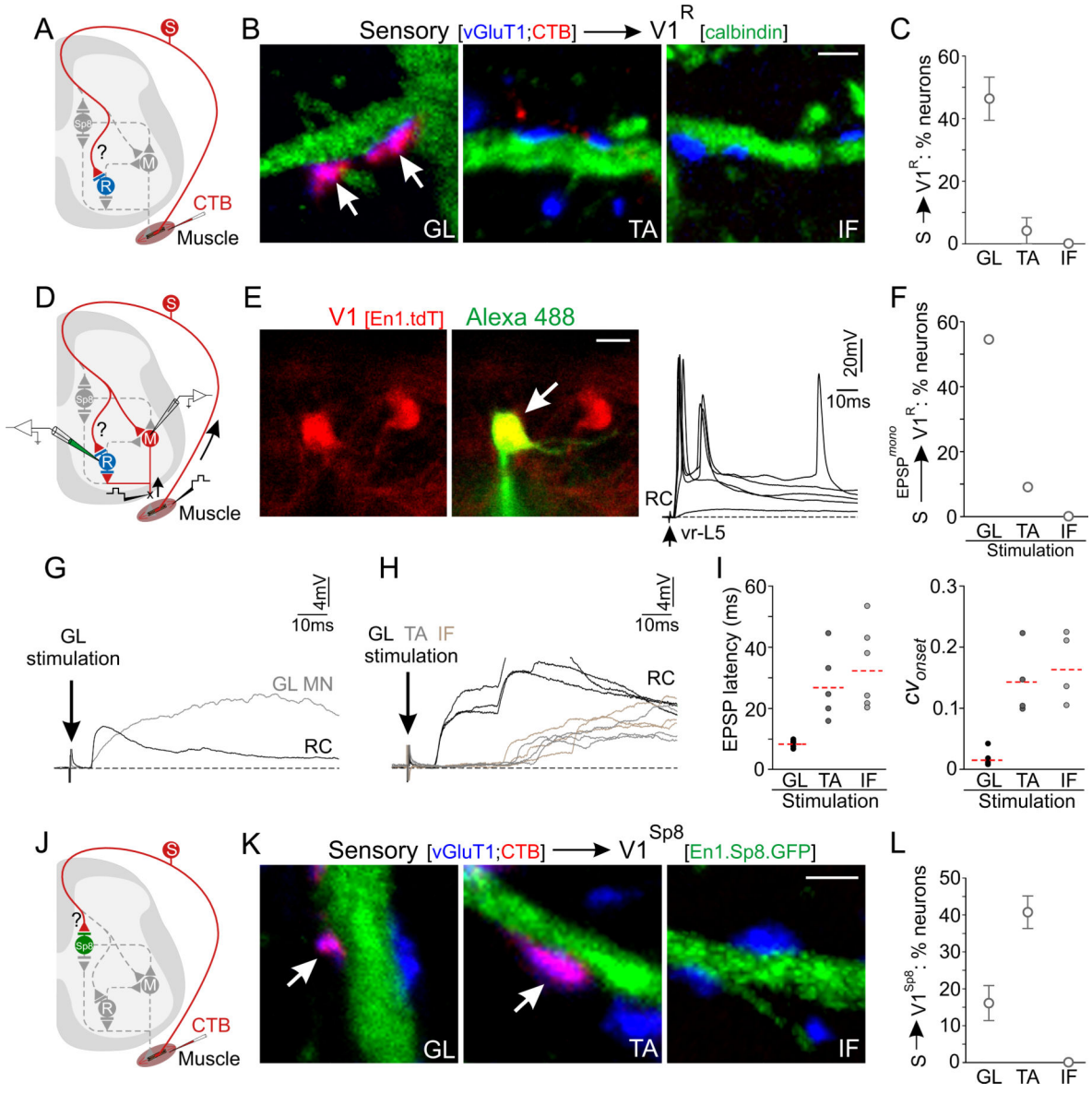

Figure 6. Specificity of Sensory-Interneuron Connectivity at Individual Joints

(A) Assay of proprioceptive input to $V1^R$ interneurons.

(B-C) CTB^+; $vGluT1^+$ proprioceptive input to $V1^R$ interneurons. (C) Percent of $V1^R$ interneurons with pool-specific input. p = 0.0007, one-way ANOVA; Bonferroni *post-hoc* test: $p < 0.01$, GL vs TA or IF, n = 3 animals. Innervation density (inputs/100 μm dendrite) for neurons receiving sensory input: GL, 5.1 ± 1.0; TA, 2.8 ± 1.9. All data are mean ± SEM. Scale bar = 2 μm.

(D) Assay of monosynaptic input from pool-specific Ia afferents onto $V1^R$ interneurons.

(E) Left, $V1^R$ interneurons (red, labeled in *En1::Cre; Rosa.lsl.tdT* mice) targeted for intracellular recording, filled with Alexa-488 hydrazide (green). Right, stimulation of L5 ventral root (vr-L5) at different intensities evoked graded short-latency synaptic potentials. Scale bar = 10 μm.

(F) $V1^R$ interneurons (GL: 6/11 cells; TA: 1/11 cells; IF: 0/11 cells) receiving monosynaptically-evoked EPSPs from peripheral muscles.
(G) Monosynaptic EPSPs in a $V1^R$ interneuron (black) or GL motor neuron (gray) following GL muscle stimulation.
(H) Short-latency EPSPs evoked in $V1^R$ interneurons after GL stimulation (3 superimposed responses evoked at 0.1 Hz stimulation frequency, black). Stimulation from TA (gray) or IF (brown) muscle sensory fibers resulted in long (>20 msec), variable latencies, indicative of polysynaptic activation. Arrow, stimulation artifact.
(I) Left, latencies from synaptically evoked responses in $V1^R$ interneurons after stimulation of GL, TA, and IF muscles in p4 to p5 mice. The latency from GL muscle stimulation was significantly shorter than from TA or IF ($p < 0.05$, one-way ANOVA). Right, coefficient of variation (CV_{onset}) of synaptic response latency. Red line = mean.
(J) Assay of proprioceptive sensory input onto $V1^{Sp8}$ interneurons.
(K-L) CTB^+; $vGluT1^+$ proprioceptive input to $V1^{Sp8}$ interneurons. (L) $V1^{Sp8}$ interneurons with pool-specific input. $p = 0.004$, one-way ANOVA; Bonferroni *post hoc* test: $p < 0.01$, GL vs TA; $p < 0.001$, TA vs IF; n.s., GL vs IF, $n \geq 3$ animals. Average CTB^+; $vGluT1^+$ input density/100 μm of $V1^{Sp8}$ dendrite: GL: 0.92 ± 0.23; TA: 2.20 ± 0.14; IF: 0 ± 0; $p < 0.0001$, oneway ANOVA; Bonferroni *post hoc* test: $p < 0.01$, GL vs TA; $p < 0.05$, GL vs IF; $p < 0.001$, TA vs IF. Similar labeling efficiency was observed for GL, TA, and IF sensory afferents (Figure S7C). Scale bar = 2 μm. See also Figure S7.

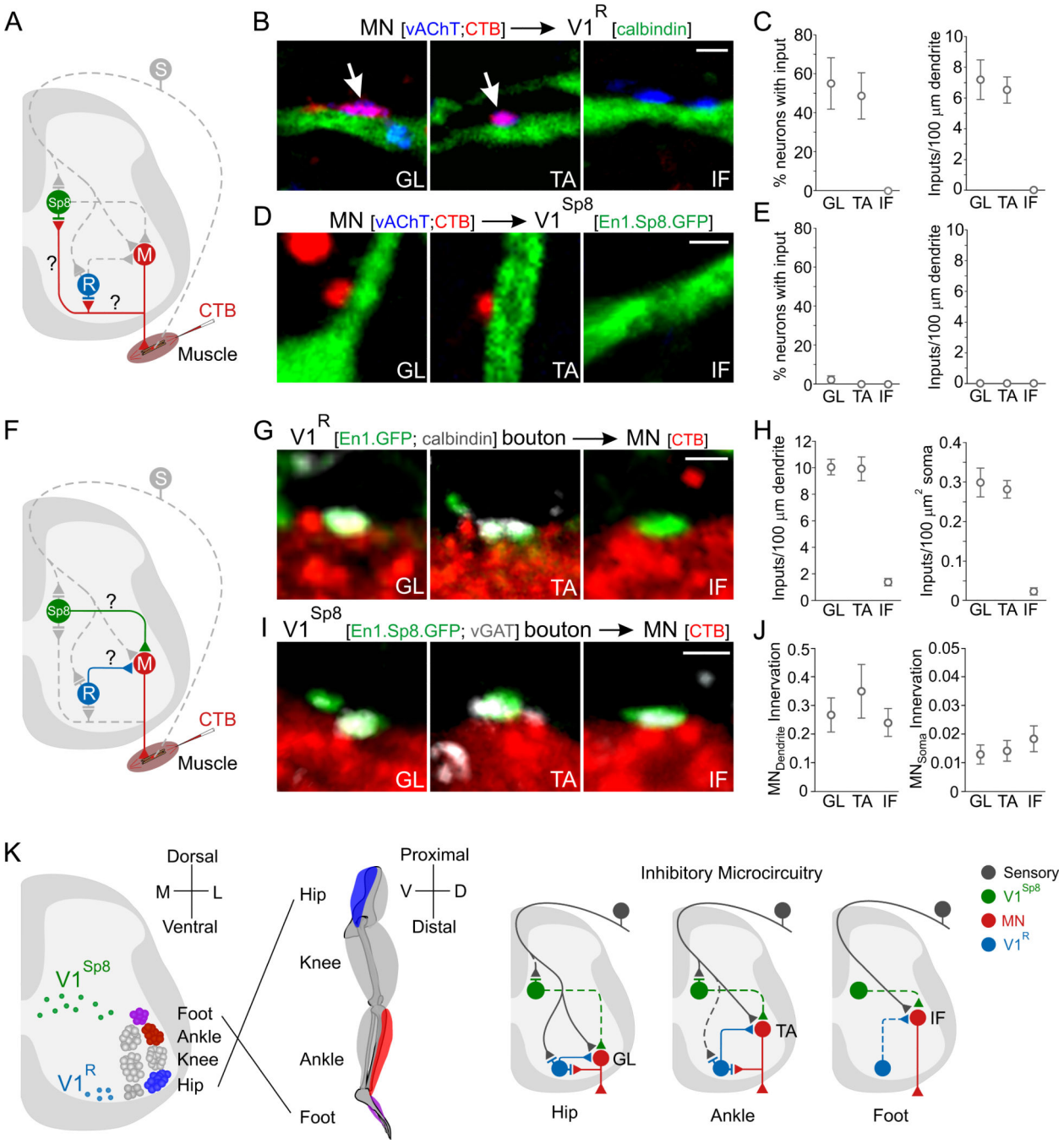

Figure 7. Specificity of Interneuron-Motor Neuron Interconnectivity at Individual Joints

(A) Assay of pool-specific motor input to interneurons.

(B-C) $V1^R$ interneurons receive CTB^+; $vAChT^+$ input from GL and TA (arrows) but not IF motor neurons (MN). Scale bar = 2 µm. (C) Left, $V1^R$ interneurons with input from GL, TA, or IF MNs. p = 0.02, one-way ANOVA; Bonferroni *post-hoc* test: $p < 0.05$, GL or TA vs IF. Right, CTB^+ MN inputs/100 µm of $V1^R$ dendrite length. p = 0.002, one-way ANOVA; Bonferroni *post-hoc* test: $p < 0.01$, GL or TA vs IF; $p > 0.5$, GL vs TA, $n \geq 3$ animals, and 23 (GL), 24 (TA), or 15 (IF) cells.

(D-E) Absence of MN input to $V1^{Sp8}$ interneurons. GL, n = 4 animals, 43 cells; TA, n = 2 animals, 52 cells; IF, n = 3 animals, 43 cells.
(F) Assay of interneuron input onto motor pools.
(G-H) $V1^{R}$ interneurons preferentially innervate GL and TA relative to IF motor pools, on proximal MN dendrites (H, left) or soma (H, right). $p < 0.0001$, one-way ANOVA; Bonferroni *post hoc* test: $p < 0.001$, GL or TA vs IF, n = 4 animals, and 31 (GL), 21 (TA), or 27 (IF) cells.
(I-J) $V1^{Sp8}$ interneurons sparsely and uniformly innervate motor pools acting on different joints. Number of $V1^{Sp8}$ inputs/100 μm MN dendrite or 100 μm^2 of soma area, normalized to $V1^{Sp8}$ interneuron number. $p = 0.53$ or 0.65 for dendrites and soma, respectively, one-way ANOVA, $n \geq 3$ animals, 35 (GL), 42 (TA), or 59 (IF) cells. Scale bars = 2 μm. All data are mean ± SEM.
(K) $V1^{R}$ and $V1^{Sp8}$ microcircuits operating on hip, ankle, and foot motor neurons. Solid and dotted lines represent prevalent and sparse synaptic connectivity. See also Figure S7.